Chemical Engineering Journal 243 (2014) 197–206

Contents lists available at ScienceDirect

Chemical Engineering Journal

journal homepage: www.elsevier.com/locate/cej

Design and operational limits of an ATR-FTIR spectroscopic microreactor for investigating reactions at liquid–solid interface

Alejo Aguirre, Pablo A. Kler, Claudio L.A. Berli, Sebastián E. Collins *

INTEC (UNL-CONICET), Güemes 3450, Santa Fe, Argentina
Instituto de Desarrollo Tecnológico para la Industria Química (INTEC), Universidad Nacional del Litoral, CONICET, Güemes 3450, S3000GLN Santa Fe, Argentina

HIGHLIGHTS

- An attenuated total reflection microfluidic cell was designed.
- Optimization of the inner flow was obtained by 3D numerical simulations.
- Transport of the reactant is characterized by convection and diffusion.
- Criteria to operate under chemical control are presented.
- CO adsorption in aqueous phase on platinum thin film is studied.

ARTICLE INFO

Article history:
Received 13 October 2013
Received in revised form 28 December 2013
Accepted 1 January 2014
Available online 8 January 2014

Keywords:
Attenuated total reflection
Infrared spectroscopy
Catalysis
Transport
Surface reaction
Fluid-dynamics

ABSTRACT

This work presents the design and characterization of an optimized attenuated total reflection (ATR) microfluidic cell to assess intrinsic kinetic parameters of reactions at the liquid/solid interface under chemical control. A theoretical and computational investigation of convection, diffusion, and adsorption is presented. Transport dynamics in transient-flow experiments is characterized by a convective and diffusive mass transport of the solution species to the surface of the ATR crystal. Criteria to determine the mass transport limitations of the adsorption process are presented as a function of the Damköhler and Biot numbers. The CO adsorption on a thin film of platinum is studied in order to validate the model.

1. Introduction

For a rational design and optimization of new efficient catalytic systems, it is crucial to understand reaction mechanisms under reaction conditions, that is, identifying and monitoring chemical species involved in the reactions and finding relationships between structure and reactivity. To this end, significant advances have been done in the *in situ* investigation of catalysts under real conditions of operation, e.g. *operando* spectroscopies [1,2].

In order to correlate chemical reactive surface species with the observed reactivity (reaction rate, apparent activation energy), the spectroscopic cell must perform as an actual catalytic reactor. In a recent review of this topic, Meunier [2] point out that spectroscopic cells are typically not ideal catalytic reactors, since a compromise must be found between (i) allowing the electromagnetic wave to probe the catalyst and (ii) keeping the bed geometry and temperature/flow control appropriate. Thus, most of the *operando* reactors have been developed for studies of reaction in the gas(reactant)/solid(catalyst) interface. For instance, several cells in diffuse reflectance infrared spectroscopy (DRIFT) [3,4], Raman [5] and X-ray absorption spectroscopies (XAS) [6] have shown to behave as plug-flow microreactors. Conversely, less developed are the spectroscopic reactors to investigate heterogeneously catalyzed reaction in liquid phase, this is probably due to the fact that all problems listed before are augmented in the condensed phase.

Attenuated total reflection (ATR) infrared (IR) spectroscopy is an appropriate tool for the investigation of reaction pathways in liquid(reactive)/solid(catalyst) systems, because it provides the detection of species adsorbed on a catalyst under reaction conditions [7]. Catalysts are usually deposited on the internal reflection elements (IRE) as films (e.g. metal film) or as layers of powders, and they are exposed to the liquid phase reactants. Usually, the presence of strongly absorbent condensate phase (solvents and

* Corresponding author. Address: INTEC-CONICET, Güemes 3450, S3000GLN Santa Fe, Argentina. Tel.: +54 3424559174.
E-mail address: scollins@santafe-conicet.gov.ar (S.E. Collins).

1385-8947/$ - see front matter © 2014 Elsevier B.V. All rights reserved.
http://dx.doi.org/10.1016/j.cej.2014.01.001

reactants), spectator species and/or the catalyst itself can make very difficult or preclude both the identification and tracking of the true active species, that is, the reaction intermediates. Then, transient experiments are widely applied in the analysis of reaction intermediates by perturbing a catalytic system working under steady state conditions (ss). Particularly, modulation excitation spectroscopy (MES) with phase sensitive detection (PSD) has proved to be an adequate methodology to study reactions in liquid/solid interfaces [7–10].

However, in most reported studies, an ATR cell is used as a qualitative technique to track surface intermediate species [7], and in some cases the measurement of kinetic data do not consider the mass-transport problems that are likely involved [11]. Therefore, to obtain quantitative information, that is, determining intrinsic reaction rates, the chemical engineering aspects of an ATR flow-through cell must be developed. Thus, to correctly extract the intrinsic kinetics information of chemical steps such as adsorption or surface reaction, mass transport in the ATR cell has to be considered. This point becomes even more important when multiple internal reflection elements (IRE) with high geometrical surface area are used in the ATR experiments in order to improve the signal-to-noise ratio. In this case the concentration may vary significantly not only with time but also in space. For instance, Baiker and co-workers [12] showed that, given the fluid dynamic characteristics of flow-through ATR cells, the mass transport phenomena are governed by a convection–diffusion mechanism. Later, Bieri and Bürgui [13] employed this model to calculated relative adsorption and desorption rates of proline on self-assembled monolayers of L-glutathione on gold by MES-ATR. Nevertheless to our knowledge no systematic and quantitative characterization of the impact of mass-transfer limitation to perform investigation in an ATR cell under kinetic control has been reported. In this work we present an optimized design of a flow-through ATR cell for transient experiments in the solid–liquid interface and an analysis of the operative limits to obtain intrinsic kinetic information under chemical control.

2. Experimental

2.1. Spectroscopic setup

A stainless steel flow-through ATR cell with small volume and minimized dead volumes was design and constructed. The cell was mounted onto an ATR attachment (Pike Technologies) inside the sample compartment of the FTIR spectrometer (Thermo-Electron, Nicolet 8700 with a cryogenic MCT detector). The bench of the spectrometer was continuously purged with dried air (Parker Balston FTIR purge gas generator) to eliminate CO_2 and water vapor contributions to the spectra. Time-resolved ATR-FTIR spectra were recorded in kinetic and rapid-scan mode at a resolution of 4 cm^{-1} (up to 1 spectrum/0.39 s). The IRE used was a 45° trapezoidal ZnSe crystal, whose dimensions are 80 × 10 × 4 mm, providing 10 internal reflections at the liquid/crystal interface.

Liquids, provided from two separate bottles, were flowed through the cell using a pulse-free peristaltic pump (Ismatec ICP4) located at the end of the cell. A pneumatically actuated three-way valve controlled by a computer software allows to switch the stream of solutions. More details of the experimental setup can be found elsewhere [10]. Carbon tetrachloride (CarboErba HPLC grade, 99%), isopropyl alcohol (Cicarelli, 99.8%), Triton X-100 (Sigma–Aldrich), and deionized water (18 MΩ) were used.

For the CO adsorption experiments, a platinum layer with a thickness of about 20 nm was prepared by vapor deposition. In order to clear the platinum layer, the coated IRE was pretreated ex situ under pure H_2 (50 cm^3/min) at 473 K for 2 h, and purged with He at the same temperature (30 min). Next the Pt/ZnSe was fitted on the ATR cell, and after purging with He, was exposed again to H_2 (5%)/He at 293 K.

Dissolved CO in water was provided from a glass saturator, at controlled temperature, where water could be saturated by bubbling CO, and flowed through the cell using a peristaltic pump located downstream.

2.2. Computational simulation

2.2.1. Modeling and simulation of the cell fluid dynamics

Designing an efficient microfluidic device firstly demands a careful knowledge of the fluid velocity filed in the transport and reaction regions. Therefore we carried out numerical simulations to study the 3D fluid streamlines in the ATR cell, mainly in the entrance/exit regions. In the framework of continuum fluid mechanics, fluid velocity $\boldsymbol{v}$ and pressure p are governed by Navier–Stokes equations [14],

$$-\nabla \cdot \boldsymbol{v} = 0 \tag{1}$$

$$\rho\left(\frac{dv}{dt} + \boldsymbol{v}\cdot\nabla\boldsymbol{v}\right) = \nabla\cdot\left[-p\boldsymbol{I} + \mu(\nabla\boldsymbol{v} + \nabla\boldsymbol{v}^T)\right] \tag{2}$$

Eq. (1) expresses the conservation of mass for incompressible fluids. Eq. (2) expresses the conservation of momentum for Newtonian fluids of density ρ and viscosity μ. Two computational domains containing the fluid were considered and are shown schematically in Fig. 1. The no-slip condition is imposed at the walls, and isothermal conditions are assumed. The flow rate through the cell was imposed by setting the appropriate velocity at the inlet. Flow profile at the inlet was chosen as uniform and relative pressure was set to zero at the outlet.

The numerical simulations presented were performed in PETSc (Portable Extensible Toolkit for Scientific Computation)-FEM (Finite Element Method), which is a parallel code primarily targeted to 2D and 3D finite elements computations, on general unstructured grids [15]. PETSc-FEM provides a set of specialized application programs addressed to a variety of multiphysics problems. In particular, fluid flow computations presented in this article were carried out within the Navier–Stokes module. Further details can be found in [16]. Visualization and post-processing were carried out in Paraview 3.6 [17].

2.2.2. Modeling and simulation of mass transfer in the cell

The 3D calculations described above demand an excessive computational time if one aims to solve the convection–diffusion transport problem of a given species in the full geometry of the cell. Instead, one may take advantage of both the large width/height aspect ratio of cell (∼14), and the fact that the flow is fully developed (see below Section 3.1), which yield a practically unidirectional flow profile throughout the cell. This suitable simplification allows one to perform accurate numerical calculations of transport phenomena in practical times.

Therefore, the following considerations are made to model the convection–diffusion problem in the computational domain shown in Fig. 2: (1) The cell operates at low Reynolds numbers (Re < 5), hence the assumption of laminar flow is appropriate; (2) the fluid velocity profile is uniform in the y-direction, and fully developed in the x-direction (except by the relatively small entry/exit zones), hence the velocity varies in z-direction only; (3) concentration variations in the y-direction are negligible small; (4) no adsorption of species on the IRE is assumed; and (5) dilute solutions are considered.

In this context, the conservation equation for the i species without chemical reaction is given by [14,18]:

$$\frac{\partial C_i}{\partial t} + \frac{\partial C_i}{\partial x}v_x(z) = D_i\left(\frac{\partial^2 C_i}{\partial x^2} + \frac{\partial^2 C_i}{\partial z^2}\right) \tag{3}$$

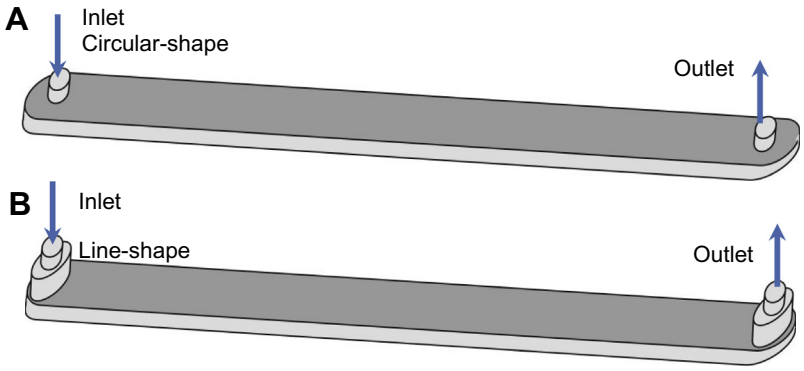

Fig. 1. Scheme of 3D flow domain used in fluid dynamic calculations. (a) Cell with circular-shape entrance/exit ports; and (b) cell with line-shape entrance/exit ports.

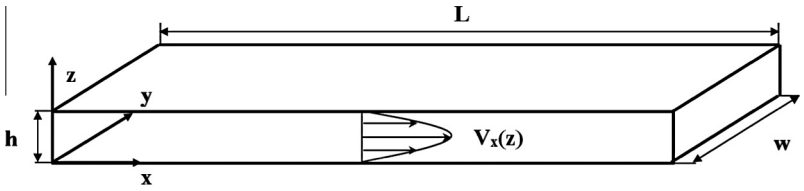

Fig. 2. Scheme of the rectangular flow cell. Simplified domain used to simulate the transport phenomena. Cell dimensions are h = 250 μm, w = 3.4 mm, L = 70.7 mm.

where C_i is the molar concentration, D_i is the diffusivity, and $v_x(z)$ is the velocity profile given by:

$$v_x(z) = 6U\left[\left(\frac{z}{h}\right) - \left(\frac{z}{h}\right)^2\right] \tag{4}$$

In Eq. (4), U is the cross-section averaged velocity, obtained as $U = Q_v/(wh)$, where Q_v is the volumetric flow rate. This flow is in steady state, and it involves the no-slip condition at the walls. For the species concentration, the boundary conditions in the flow domain of Fig. 2 are:

For $t > 0$:

$$z = 0 \quad \frac{\partial C_i}{\partial z} = 0 \tag{5}$$

$$z = h \quad \frac{\partial C_i}{\partial z} = 0 \tag{6}$$

$$x = 0 \quad C_i = C_i^0 \tag{7}$$

$$x = L \quad \frac{\partial C_i}{\partial x} = 0 \tag{8}$$

The initial condition for the species i is:

$$t = 0 \quad 0 \leqslant x \leqslant h,\ 0 \leqslant z \leqslant L,\ C_i = 0 \tag{9}$$

The set of Eqs. (3)–(9) were numerically solved by using the finite differences method implemented in Octave GPL software [19].

Finally, it is worth to remember that the signal recorded in the ATR cell only senses the fluid volume in the close vicinity of the IRE, due to the exponential decay of the evanescent wave. In order to compare the numerical simulations with experimental results, the normalized concentration of the solute i has to be calculated by means of the following equation [20],

$$A_N(\lambda, t) = \frac{2}{Ld_p}\int_0^L\int_0^h \frac{C_i(x,z,t)}{C_i^0} e^{-2z/d_p}\,dz\,dx \tag{10}$$

where $A_N(\lambda, t)$ is the normalized absorbance relative to the maximum concentration C_i^0 and d_p is the penetration depth of the evanescent wave [20], which is given by:

$$d_p = \frac{\lambda}{2\pi n_1\sqrt{\sin^2\theta - \left(\frac{n_2}{n_1}\right)^2}} \tag{11}$$

In this expression, n_1 is the refractive index of the IRE, n_2 the refractive index of the sample, θ is the incidence angle and λ is radiation wavelength.

Besides, Eq. (10) is normalized in the cell length L because a multi-bounce ATR cell is used to enhance the signal from the species in whole surface of the IRE element. Therefore, once the species concentration in the cell domain is obtained through Eqs. (3)–(9), the IR normalized absorbance is readily calculated from Eq. (10).

3. Results and discussion

3.1. Design and optimization of a flow-through ATR microfluid cell

A flow-through ATR cell in which kinetic analysis of adsorption and reaction can be performed was designed with the following criteria: (a) the volume of the cell should be small enough to allow rapid exchange of the reactants without dead volumes, (b) the fluid velocity and the profiles of concentration into the cell should be as uniform as possible to simplify data analysis. Particularly, the geometry of the inlet and outlet ports, as well the height of the cell, had to be optimized to avoid dead volumes and prevent backflow zones.

A critical aspect in the design of a flow-through ATR cell are the inlet/outlet ports due to the physical limitations imposed by the fitting of the IRE to the cell body. Thus, two main configurations are possible: (i) one inlet tube connected to one commutation valve upstream, and (ii) two independent tubes, each one with its own valve connected to the entrance orifice leading to the interior of the cell. The last option was used in the ATR cell presented by Urakawa et al. [12]. That cell allows minimizing the exchange times, since practically there is no volume previous to the "sensor" part of the cell. However, in that configuration, after switching the flowing liquid remains in contact, through the shared entrance, with the stagnant one with the possibility of diffusion of solvent

or solute into the cell and hence cross-contamination of the catalyst. On the other hand, the first configuration, which was the one adopted in our design, allows circumventing problems of cross-contamination due to the use of one valve to exchange reactants. Although, it produces a lag in inlet of reactants into the cell due to the tube connected to the cell, this lag time can be systematically corrected, as will be discussed later. Additionally, into the connecting tube a mixing of reactants could occurs. We have run simulations and concluded that this problem can be neglected in comparison with the time needed to exchange the solute in the ATR cell (for more details see Supplementary Information).

In order to optimize the dimensions of the cell, a series of 3D simulations of the flow was carried out. These simulations showed that a circular-shape entrance/exit causes a significant distortion in the flow due to low flow rates in the regions close to the axial extremes of the cell. Fig. 3a shows the simulation using that geometrical configuration (usually used in commercial and research ATR cells). As can be seen in the figure, streamlines take radial paths at the exit of the port, with large fluid velocities towards the center of the cell, and a slow backflow at the ends. This produces a distorted concentration profile in the transverse direction of the cell, and also let to a high exchange time. To circumvent these issues, the optimized design (Fig. 3b) includes line-shaped entrance and exit ports, placed as close as possible to the ends of the cell. In this way back flows were minimized, hence the fluid velocity is quite uniform across the cell, and fully developed immediately after the ports.

On the basis of this optimized design, an ATR cell was micromechanized in 316L stainless steel. The cell has three main parts (Fig. 4a): (i) the top body with a drilled liquid-jacket to allow the control of the temperature of the cell by means of a thermostatized water bath (±0.5 K), a cavity to host a Viton O-ring which define the height of the cell, and the inlet and outlet ports with the before described geometry; (ii) the lower body, where the IRE is adjusted to the O-ring defining a total cell volume of 60 μL (3.4 × 0.25 × 70.7 mm); (iii) pieces to locate the mirrors to focus the IR beam (more details of the cell are present in Fig. S1 in Supplementary Information). The inlet and outlet have zero-volume fittings (Vici-Valco) to connect the 1/16″ tubes to the 3-way valve that allow exchange of the fluids (Fig. 4b). The cell is fitted with a 45° trapezoidal IRE whose dimensions are 80 × 10 × 4 mm, providing 10 internal reflections at the liquid/crystal interface. Experiments presented here were performed with a ZnSe crystal.

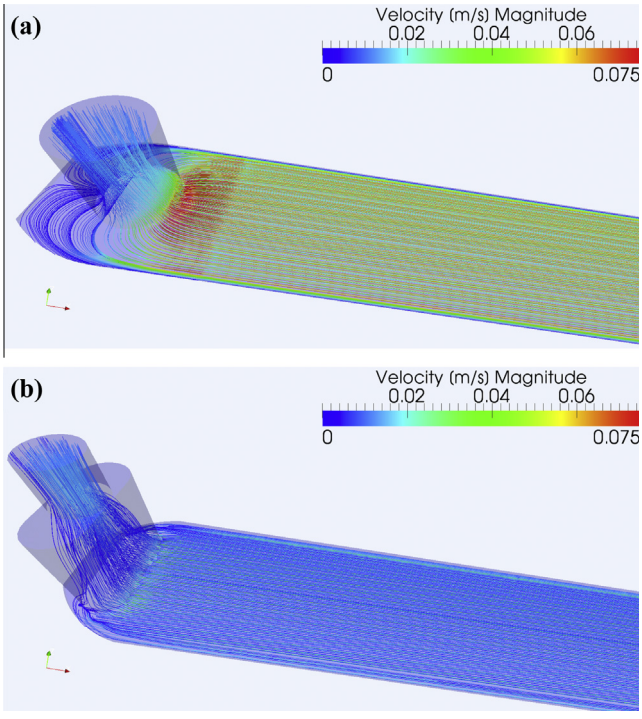

Fig. 3. 3D fluid streamlines at the entrance/exit of the cell, for water at room temperature. Plotted lines are those corresponding to the midplane of the cell. (a) circular-shape entrance port, 1 mm i.d., and (b) linear-shaped entrance port, 1 × 3 mm. Flow rate, Q_v = 1 mL/min.

3.2. Mass transport characterization

Firstly the fluid dynamic behavior of the cell was experimentally probed by studying the exchange of two mutually insoluble liquids: water and carbon tetrachloride. Fig. 5 presents the evolution of the integrated IR signal of water [δ(OH) = 1640 cm^{-1}] after switching at three flow rates Q_v = 0.8, 1.5 and 2.2 mL/min. In this case, the surface tension forces domain and one fluid pushes the other across the cell length, with a velocity equal to the mean velocity $U = Q_v/S$, where S is the cell cross sectional area. Zero time is set when the valve is switched. Considering the geometric volume of the cell, 60 μL, the expected residence times ($\tau = LS/Q_v$) for the three flow rates are 4.5, 2.4 and 1.6 s, respectively. As shown in Fig. 5, the experimentally obtained residence times are in good agreement with the expected ones. There is a delay in the observed signal due to the volume between the valve and the cell. This experiment allowed correcting the time delay in following measurements. In contrast, the commercial cell used as reference, which has a volume estimated in 500 μL showed a very long time of exchange and also the impossibility to completely exchange water/tetrachloride due to the presence of important dead volumes (see Supplementary Information Fig. S2).

The transport phenomena in the cell were experimentally examined, by following the IR signals during the exchange of pure water to a solution containing solutes with relatively low and high diffusion coefficients. Results are compared to the theoretical predictions obtained by numerical simulations, which were carried out for Triton X-100 ($D_M = 5.5 \times 10^{-7}$ cm^2/s [21]) and isopropyl alcohol ($D_M = 0.8 \times 10^{-5}$ cm^2/s [22]).

Transient experiments were performed by changing pure water to aqueous solution containing isopropyl alcohol (0.65 M) or Triton X-100 (0.086 M), for Q_v = 0.8, 1.5 and 2.2 mL/min, by using the optimized cell, and the commercial cell as a reference. Time-resolved IR spectra were collected (1 spectrum/0.39 s) to register details during the transient exchange. Fig. 6 shows the evolution of the selected IR signal [ν(COC) = 1097 cm^{-1}] of Triton X. The corresponding figures for isopropyl alcohol [ν(CO) = 1126 cm^{-1}] are reported in Supplementary Information Section for the sake of brevity (Fig. S4).

Data from the commercial ATR cell clearly shows that very high exchanging times are needed to fill and empty the cell due to its big volume and non-uniform flow profile (see Fig. S5). In contrast, the optimized cell shows a rapid exchange of both solutes (Fig. 6). However, after correction of the delay time, it can be noticed that the time to exchange each solution is clearly longer than the residence times shown before (Table 1). This behavior indicates that some transport limitations are taking place in the cell [12]. Note again that the IR beam is only sensing ca. 2 μm of the fluid above the IRE.

Fig. 7 shows snapshots calculated at different times during the solvent/solution exchange for Triton X solution (isopropyl alcohol is shown in Fig. S6). As seen in the figures, the slow fluid velocity in the bottom and top as compared with the center of the cell makes that the solute takes a longer time to reach the steady state concentration of the species i. Then, the swept of the solute is

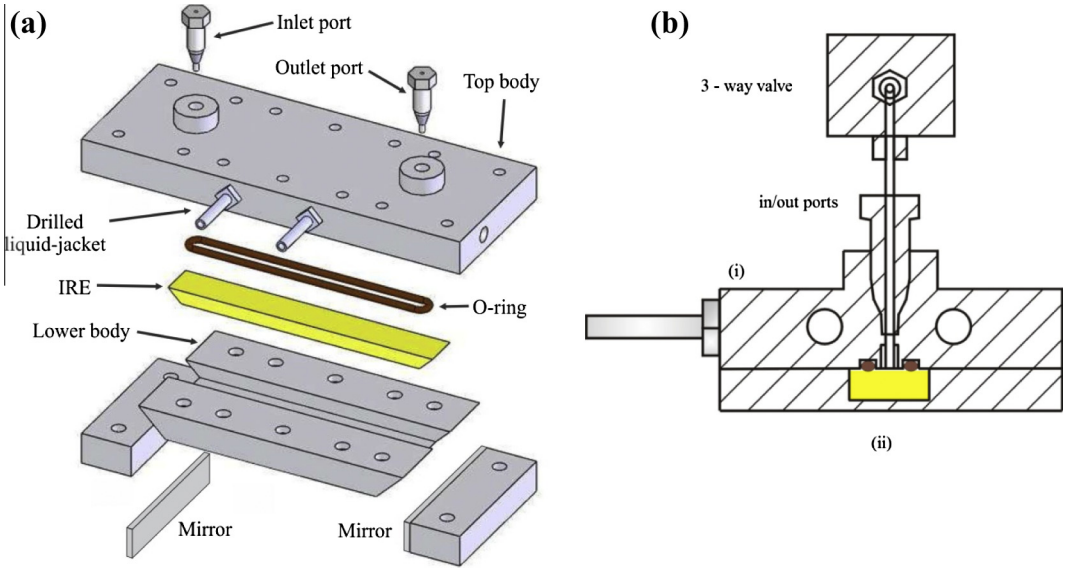

Fig. 4. (a) Scheme of the main parts of the ATR cell (see text); and (b) details of the entrance/exit ports.

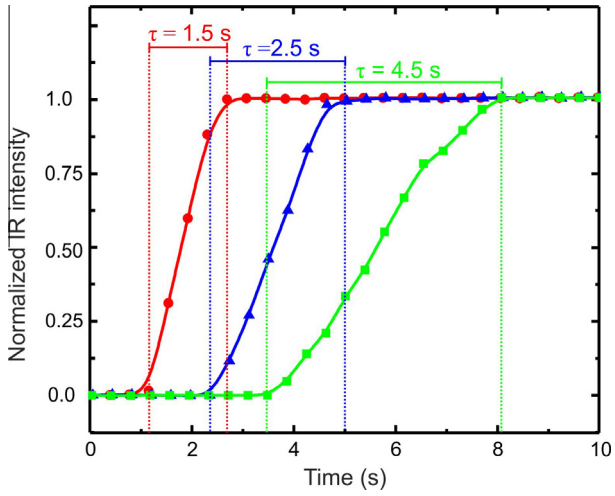

Fig. 5. Normalized IR signal of water [δ(OH) = 1640 cm^{-1}] after switching from CCl_4 to H_2O at Q_v = 0.8 (squares), 1.5 (triangles) and 2.2 mL/min (circles). The residence time of the cell (τ) is calculated as the time at which the IR signal reaches the maximum intensity minus the signal delay time.

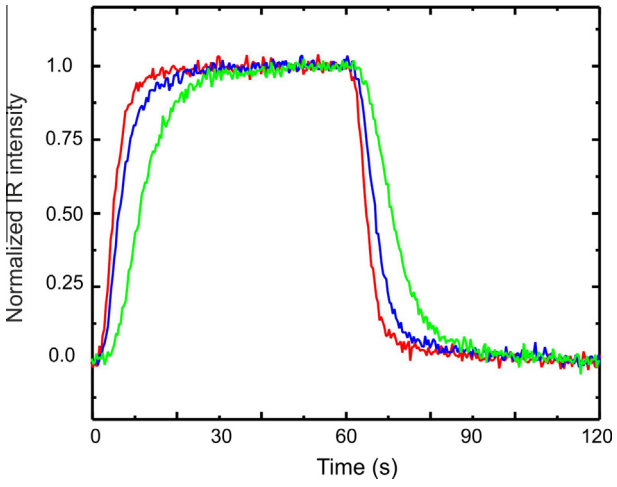

Fig. 6. Evolution of the IR signal of Triton-X [ν(COC) = 1097 cm^{-1}] into the optimized ATR cell for Q_v = 0.8 (green line), 1.5 (blue line) and 2.2 mL/min (red line). (For interpretation of the references to color in this figure legend, the reader is referred to the web version of this article.)

governed by the diffusion. Similar results were reported by Urakawa et al. [12].

The isopropyl alcohol and Triton X responses of the experiments measured by ATR and the convection–diffusion model considering the penetration depth of the evanescent wave are compared in Fig. 8 at different flow rates. As seen in the figures, the agreement between the experimental results and the model is excellent and only minor deviation (<5%) observed at the exit of the cell due to the effect of the inlet and outlet ports, which are not considered in the 2D model.

The difference in the times required to attain the steady state concentration between isopropyl alcohol and Triton X solutions can be attributed to the lower diffusion coefficient in the last one. These results show that the optimized ATR-FTIR flow cell enables a rapid exchange of fluid, but the time necessary to reach a homogeneous concentration near the IRE, where the catalyst is deposited, is transport-limited by a convection–diffusion regime.

It is important to notice that this is a general problem in any ATR cell, mainly in cells without an optimized flow design, which is commonly not taken into account when kinetics measurements are performed [12].

Table 1
Comparison of the exchange time of different solutes with the residence time of a fluid volume equivalent to the geometric cell volume.

Flow rate (mL/min)	2.2	1.5	0.8
Residence time[a] (s)	1.6	2.5	4.5
Exchange time isopropyl alcohol[b] (s)	9.0	13.5	18
Exchange time Triton-X[b] (s)	14	20	26

[a] Obtained from Cl_4C/H_2O exchange.
[b] Exchange time calculated as the time at which the IR signal reaches 99% the maximum intensity (average of the experimental points) minus the signal delay time.

3.3. Assessment of the operative limits

The determination of intrinsic reaction rates require that the chemical engineering aspects of operando reactors be fully

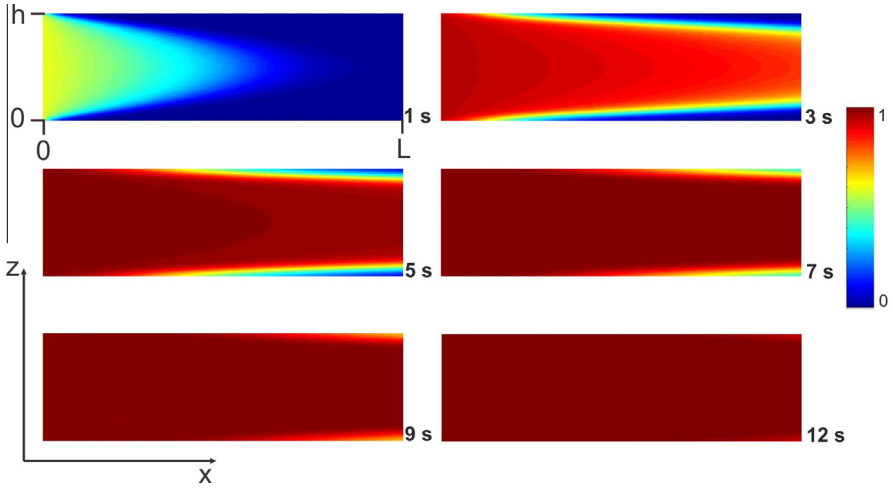

Fig. 7. Time-resolved snapshots of the convection–diffusion model predictions for the exchange of water to Triton X-100 solution.

considered. As stated in the introduction section, the aim of the optimization of an ATR cell is to be able to measure kinetic process at liquid/solid interfaces, such as adsorption and surface reactions in heterogeneous catalysis. In this sense, the obtained data in transient experiments of this kind should be under chemical control that is, ideally, free of mass transport limitations. However, as was proved before, a diffusion-convection regime governs the transport of the reactants to the surface of the IRE where the catalyst would be deposited. Therefore, operational limits should be determined. Recently, a similar problem has been addressed by Gervais and Jensen [23] and Hansen et al. [24] for the appropriate operation of surface-based sensors in microfluidic system based on surface plasmon resonance (SPR). It is worth noticing here that, unlike SPR devices, an ATR cell allows one the simultaneous measurement of the bulk concentration of the reactant(s) – at least near the IRE- and the adsorbate coverage bounded to the surface sites [7].

Next we analyze the simplest case, that is, the molecular (non-dissociative) adsorption–desorption process in a non-porous layer. The equation that describes the evolution of the surface concentration, $\Gamma(x, t)$, with is:

$$\frac{\partial \Gamma}{\partial t} = k_a C_i^w(\Gamma_0 - \Gamma) - k_d \Gamma \tag{12}$$

where k_a and k_d are the adsorption and desorption (independent of the coverage), C_i^w is the concentration of the solute at the catalyst surface ($z = 0$), and Γ_0 is the total number of binding sites. Note that, as stated before, no concentration gradient is supposed in the y-direction. Ideally, in an ATR flow cell the concentration near the IRE is identical to the bulk concentration at any time subsequent to the time needed to completely exchange the reactant, which means true chemical control without resistance to mass transfer. If this occurs, Eq. (12) can be easily solved to give

$$\ln\left(1 - \frac{\theta}{\theta_\infty}\right) = -(k_a C_i^0 + k_d)t \tag{13}$$

where $\theta = \Gamma/\Gamma_0$ is the relative coverage, and θ_∞ is the coverage at steady state. Thus the ratio $\frac{\theta}{\theta_\infty}$ as a function of time is obtained. Fitting the experimental data with Eq. (13) allows one to obtain k_a and k_d, since the equilibrium constant $K_{eq} = k_a/k_d$ is available from the adsorption isotherm also measured in the same ATR cell [25–28].

When mass transport limitation are present, the observed surface concentration, $\theta(t)$, involves information of the chemical kinetic process as well the diffusion process. In that case, Eq. (12) must be solved numerically with Eqs. (3)–(9), by replacing the boundary condition (5) by

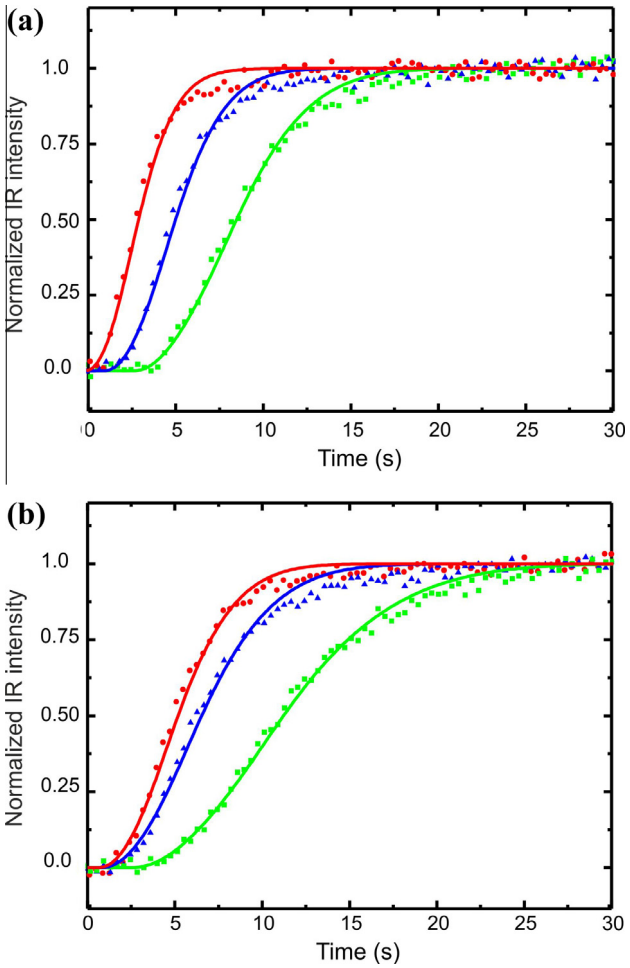

Fig. 8. Normalized IR signal as a function of time for (a) the exchange from pure water to isopropyl alcohol solution [ν(CO) = 1126 cm^{-1}], and (b) the exchange from pure water to Triton X solution [ν(COC) = 1097 cm^{-1}], at different flow rates: 0.8 (green lines), 1.5 (blue lines) and 2.2 (red lines) mL/min. Symbols are experimental data, lines are the prediction of the convection–diffusion model. (For interpretation of the references to color in this figure legend, the reader is referred to the web version of this article.)

$$z = 0,\ D_i \frac{\partial C_i}{\partial z} = \frac{\partial \Gamma}{\partial t} \tag{14}$$

and with the following initial condition:

$$t = 0,\ 0 \leqslant x \leqslant L,\ \Gamma = 0 \tag{15}$$

In order to simplify the analysis of the different variables that affect the operative performance of ATR cell, a dimensionless analysis can be carried out. Thus, the mass balance for species i takes the form,

$$\frac{\partial C_i^*}{\partial \tau} + \alpha \cdot Pe \cdot v_\eta^*(h^*) \cdot \frac{\partial C_i^*}{\partial \eta} = \alpha^2 \cdot \frac{\partial^2 C_i^*}{\partial \eta^2} + \frac{\partial^2 C_i^*}{\partial h^{*2}} \tag{16}$$

where $C_i^* = \frac{C_i}{C_i^0}$; $\tau = \frac{D_i}{h^2} t$; $\eta = \frac{x}{L}$; $h^* = \frac{z}{h}$; $v_\eta^*(h^*) = 6(h^* - h^{*2})$; $\alpha = \frac{h}{L}$ is a geometric factor; and $Pe = \frac{Uh}{D_i}$ is the Péclet number, which represents the ratio between the characteristic velocities of convective and diffusive processes. In addition, the coverage equation is

$$\frac{\partial \theta}{\partial \tau} = \beta \cdot Bi[C_i^*(1-\theta) - \overline{K_D}\theta] \tag{17}$$

where $\beta = \frac{C_i^0 h}{\Gamma_0}$ is the relative adsorption capacity; $Bi = \frac{k_a \Gamma_0 h}{D_i}$ is the Biot number; and $\overline{K_D} = \frac{k_d}{k_a C_i^0}$ is the dimensionless equilibrium desorption constant. The corresponding boundary condition is,

$$h^* = 0,\ \frac{\partial C_i^*}{\partial h^*} = \frac{1}{\beta} \frac{\partial \theta}{\partial \tau} \tag{18}$$

The relative adsorption capacity β is the ratio between the bulk concentration and the fully saturated surface coverage, that is, a small β lead to longer saturation times. The Biot number represents the ratio between the adsorption rate and the diffusivity of the reactant. When $Bi \ll 1$, the transport is limited by the reaction at the surface, while at $Bi \gg 1$ the transport becomes diffusion-limited [24]. However, this dimensionless number does not take into account the convective transport. Then, the Damköhler number, $Da = \frac{k_a \Gamma_0}{k_l}$, is a better representation of the ratio between the rate of adsorption and the flux of reactant from the bulk to the (reactive) surface considering both diffusion and convection [24]. In this expression, k_l is the mass transport coefficient defined by [14,24],

$$k_l = 1.2819 Pe^{1/3} \frac{D_i}{L^{1/3} h^{2/3}} \tag{19}$$

Thus, the Damköhler number is related to both the Biot and Péclet numbers as follows

$$Bi/Da = 1.2819(\alpha Pe)^{1/3} \tag{20}$$

A reasonable experimental condition, considering the usual propagation of errors involved in the experimental measurement in a ATR cell, could be that the observed rate deviates less than 10% from the theoretical value [29], then this criteria requires that the concentration of the reactant A at surface ($z = 0$) should be at least the 90% of the bulk concentration for a kinetic control. In that case, the Damköhler number should be lower than 0.1. Considering this criterion, it is possible to identify the range of operative conditions that can be applied to measure kinetic parameters in our ATR cell. As an example, the transport model with adsorption was solved numerically with typical parameters taken from the literature for adsorption of proteins [30,31]: $D_A = 1 \times 10^{-10}$ m^2 s, $\Gamma = 70$ fmol/mm^2, $C_A^0 = 1$ μM, $K_e q = 1 \times 10^8$ M^{-1}. The flow rate was $Q_v = 2.2$ mL/min, leading to $Pe \approx 10^5$. Table 2 summarizes the parameter values used in calculations.

Fig. 9 shows the bulk concentration of the adsorbate for different Damköhler numbers, and different positions along the x-direction (near the entrance and near the exit). The concentration profiles are taken at $t = 12.5$ s, that is, when the bulk and surface concentration reaches a steady state in a blank experiment (without adsorption). As seen in Fig. 9, the concentration gradient in the z-direction increases with Da. For $Da = 0.093$, only a slightly concentration gradient is observed, which enable measurements under the kinetic control, in agreement with the pre-fixed criteria (wall concentration is a 90% of the bulk concentration).

Table 2
Parameters employed for the simulations and corresponding Bi and Da numbers.

Simulation	1	2	3
k_a (M^{-1} s^{-1})	5×10^3	5×10^4	5×10^5
Da	0.093	0.93	9.3
Bi	0.875	8.75	87.5

ATR technique allows to distinguish a condition where important mass transport problems are present due to the simultaneous observation of the IR signal of the adsorbate in solution and bonded to the surface. Fig. 10 compares the time evolution of the surface coverage without mass transport limitation and with a 10% of deviation ($Da = 0.093$). There, almost identical profiles are observed. However, from a practical point of view, when studying an unknown system the time response of the concentration of the adsorbate in solution registered by IR during the transient experiment provides a more straightforward information. Fig. 11 shows the calculated evolution of the normalized concentration of the adsorbate in solution seen by the IR beam in a blank experiment and using with the Damhköler numbers from Table 2. As shown before, in the transient experiment without adsorption a steady state concentration is reached at ca. 12 s. Then, deviations from this profile increases as the Damhköler number does, indicating the presence of mass transference problems.

To summarize, Fig. 12 includes the Biot number as a function of the Péclet number, which allows one to define an operational zone where kinetic control is assured, under the adopted criteria. The lower line corresponds to $Da < 0.1$, as required to fulfill the chemical control regime where the observed rate is 90% of the real one. At higher Da numbers, an intermediate regime is found where the observed reaction rate is influence by both intrinsic kinetics as well as mass-transfer. In this zone, kinetic parameters can also be obtained by solving numerically the full model.

Finally, in the highest part of the plot, mass-transport controls the process and it is impossible to obtain kinetic values (diffusive

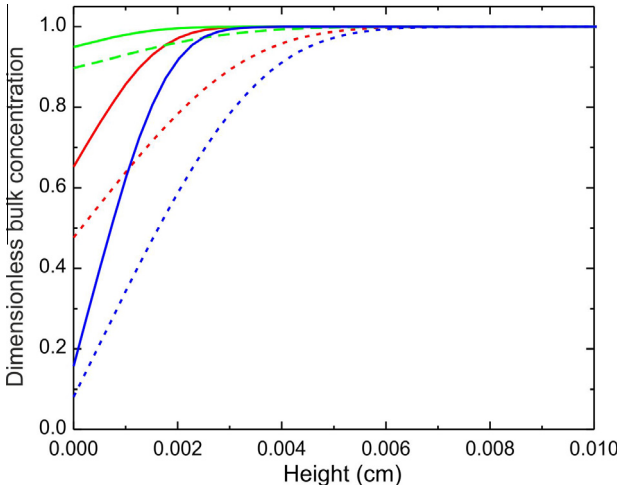

Fig. 9. Dimenssionless bulk concentration of the adsorbate A (C_A^*) at $t = 12.5$ s, as a function of the cell height, for different positions along the x-direction, near the entrance (1 cm, full lines) and near the exit (7 cm, dotted lines). Colors refer to Damköhler numbers: green, 0.093; red 0.93 and blue, 9.3. (For interpretation of the references to color in this figure legend, the reader is referred to the web version of this article.)

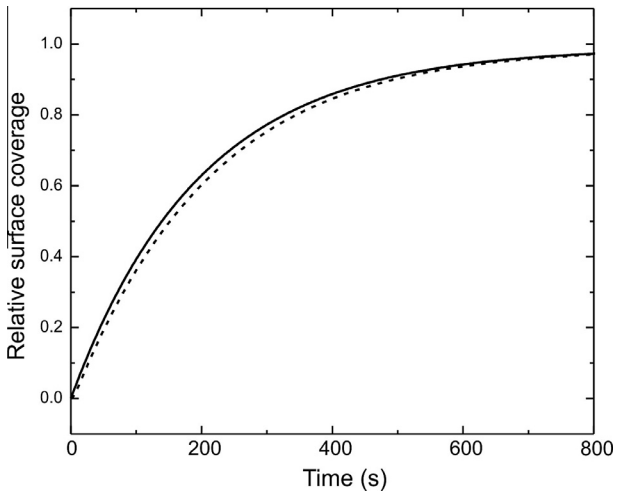

Fig. 10. Relative surface coverage as a function of time, for adsorption reaction without mass-transfer limitation (full line), and with *Da* = 0.093 (dotted line).

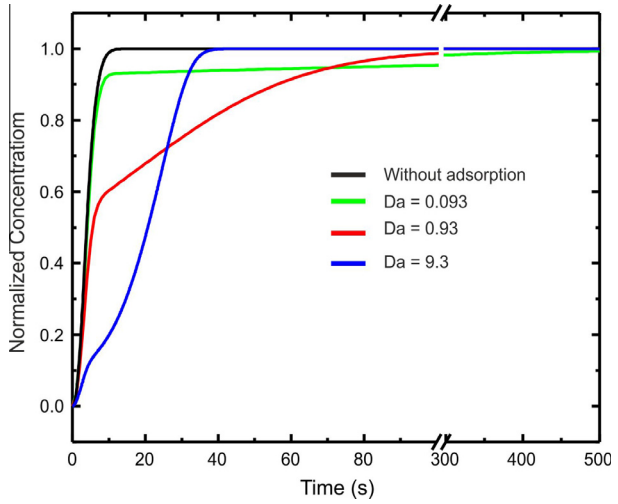

Fig. 11. Calculated normalized concentration of the adsorbate in solution seen by the IR beam in a blank experiment and using the Damhköler numbers from Table 2.

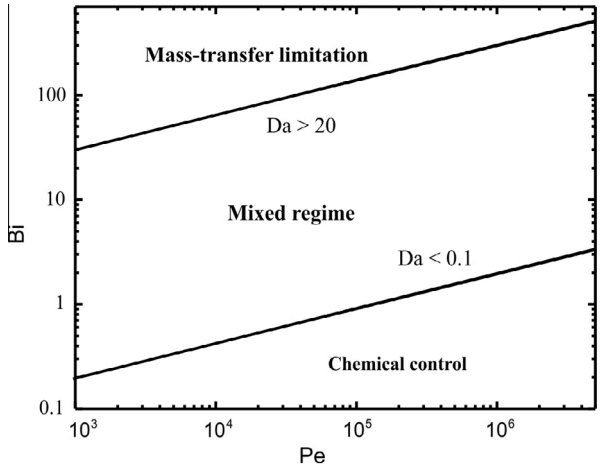

Fig. 12. Operative limits for the ATR cell defined in a Biot-Péclet numbers diagram, by using limiting Damköhler numbers as criteria to differentiate mass transport regimes.

control). This graphic chart serves as a practical guide to determine the operational limits of an ATR cell.

3.4. Case of study: CO adsorption on a Platinum thin film

As an example of the use of our optimized ATR cell and the developed criteria, results of the adsorption of CO on a platinum layer deposited on a ZnSe IRE are presented.

Time-resolved IR spectra were acquired during the CO/H_2O flow into the cell (Fig. 13, inset). Infrared peak at 2048 cm^{-1}, assigned to linear or on-top Pt–CO, increased its intensity until saturation was reached. Also, a very low signal at 1810 cm^{-1} due to bridged CO was detected, but the following analysis is focused on the linear Pt–CO. The integrity of the platinum film was verified by comparing the intensity after saturation for the IR signal of adsorbed CO in liquid phase with the one register after flowing CO(5%)/He gas on the fresh film (see Fig. S7).

The normalized integrated absorbance, representing the fractional coverage of Pt–CO, as a function of time is presented in Fig. 13 for a flow rate of 2.0 ml/min ($Pe = 5.2 \times 10^3$). The number of adsorption sites was assumed to be 10^{15} sites/cm^2, the CO concentration was 9.3×10^{-4} mol/L and the diffusion coefficient of CO in water, D, equal to 1.93×10^5 cm^2/s (calculated with the Stokes–Einstein equation [14]).

The shape of the registered curve cannot be fitted using Eq. (12) (see Fig. S8). The shape of the adsorption curve is similar to the one reported by Ferri et al. [32] and Ebbesen et al. [33] using ATR to study the adsorption of CO on platinum films. That is due to CO adsorption on platinum depends on the coverage. Usually, a Tempkin isotherm, that is a linear variation of the heat of adsorption (E) with the coverage, is used to represent the adsorption of CO on platinum. For instance, Bianchi and co-workers reported a $E(\theta = 0) = 200$ kJ/mol and $E(\theta = 1) = 115$ kJ/mol in platinum supported catalysts by means of variable temperature infrared spectroscopy to measure the isobaric heats of adsorption [34]. Likewise, the stinking coefficient, or in other words the rate of adsorption, also has been reported to be linearly dependent of the coverage [35]. Then, in this case, the evolution of the surface concentration for the irreversible adsorption of CO takes the form [35]:

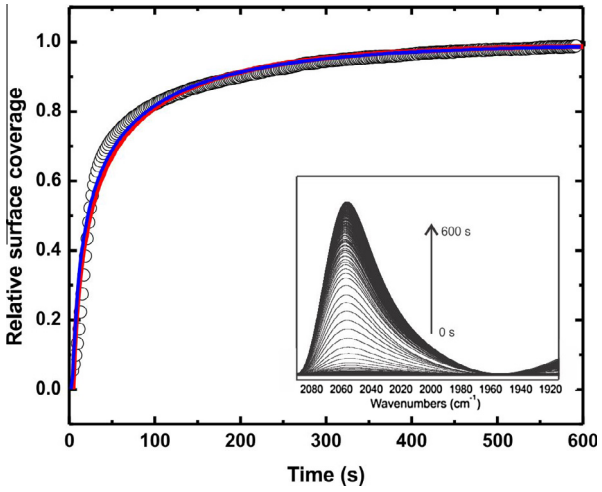

Fig. 13. Evolution of the normalized IR signal of Pt–CO (2048 cm^{-1}) as function of time. Lines are the best fitting of the data considering the complete convection–diffusion model (blue line) and only Eq. (21) (red line). For the complete model the results are: $k^0_{ad} = 104 \pm 11$ M^{-1} s^{-1} and $\alpha = 7.6 \pm 3.1$ kJ/mol. Solving the differential equation are: $k^0_{ad} = 80 \pm 17$ M^{-1} s^{-1} and $\alpha = 6.7 \pm 2.7$ kJ/mol. (For interpretation of the references to color in this figure legend, the reader is referred to the web version of this article.)

$$\frac{d\Gamma_{CO}}{dt} = \left[k_{ad}^{0} \cdot \exp\left(-\frac{\alpha\frac{\Gamma_{CO}}{\Gamma_0}}{RT}\right)\right] \cdot C_{CO}^{0}(\Gamma_0 - \Gamma_{CO}) \quad (21)$$

where the term between brackets stand for the variation of the k_{ad} with the coverage. k_{ad}^{0} is the adsorption rate at coverage zero, C_{CO}^{0} is the concentration of dissolve CO, Γ_0 is the total number of sites, Γ_{CO} is the surface coverage of CO and α is the sticking factor.

The adsorption of CO on platinum at 298 K is irreversible. After saturation, the cell was purged with pure water and the signal of Pt–CO remains stable for more than 3 h. This result confirms the high stability of the adsorbed CO on platinum at room temperature and justify that the desorption rate can be considered as zero ($k_d = 0$).

Note here, that the above adsorption model is equal to Eq. (12) at low coverage, were k_{ad} is a maximum. With the aim to estimate the influence of mass transport in the kinetic process using the criteria described in Section 3.3, the k_{ad} at initial coverage was calculated, that is, the more demanding condition. The k_{ad} ($t = 0$) obtained by fitting the experimental data was 60 M^{-1} s^{-1}. Then, the *Bi* and *Da* numbers are: 0.13 and 0.037, respectively. These results show that under this experimental condition the criteria for chemical control are fulfilled. Fig. 13 shows the fitting of the experimental data using only the differential Eq. (21) and the complete diffusion-convection model coupled with Eq. (21). As can be seen from the figure, the fitting of the data is satisfactory with both models, confirming that adsorption process is under chemical control.

4. Conclusions

Full 3D simulations of the streamlines allowed the optimization of a flow-thought attenuated total reflection (ATR) cell for the investigation of surface reactions. Linear-shaped entrance and exit ports, close to the extremes of the cell, avoid dead-volume zones and permits an uniform fluid velocity profile across the cell, which fully developed immediately after the ports.

The optimized cell was constructed and theoretical and experimentally characterized. Time-resolved IR spectra showed details of the exchange of solutions into the cell, whose evolution could be correctly described by a convection and diffusion transport model.

The mass-transfer limitation in the ATR cell was investigated using the simplest case of adsorption in a non-porous surface. The analytical solution of the transport model for an adsorption was carried out by means of the nondimensional analysis in terms of Péclet, Biot and Damköhler numbers. A suitable criteria to determine kinetic parameters under chemical control, was develop considering the geometry and experimental flow rates of the constructed ATR cell.

As a proof of the utility of the cell and the criteria for mass transport limitation, the CO adsorption was investigated on a Pt thin film deposited on the IRE. By fitting the experimental data, it is demonstrated that the operative conditions employed in the ATR cell determines the possibility of extracting useful kinetic data.

It is expected that the development of quantitative models of spectroscopic microreactors allows the determination of true reaction rates of surface reactions that improves the capabilities of operando methodology.

Acknowledgments

Financial support from the Consejo Nacional de Investigaciones Científicas y Técnicas (CONICET), Universidad Nacional del Litoral (UNL) CAIDJ379 and 0100; and Agencia Nacional para la Promoción de la Ciencia y Tecnología of Argentina (ANPCyT) PICT-729 and PME-611 is gratefully acknowledged. A.A. thanks CONICET for the fellowship received to carry out this work. The authors thank Dr. Koropecki for his help in the deposition of platinum on ZnSe.

Appendix A. Supplementary material

Supplementary data associated with this article can be found, in the online version, at http://dx.doi.org/10.1016/j.cej.2014.01.001.

References

[1] M.A. Bañares, Operando methodology: combination of in situ spectroscopy and simultaneous activity measurements under catalytic reaction condition, Catal. Today 100 (2005) 71–77.
[2] F.C. Meunier, The design and testing of kinetically-appropriate operando spectroscopic cells for investigating heterogeneous catalytic reactions, Chem. Soc. Rev. 39 (2010) 4602–4614.
[3] F.C. Meunier, A. Goguet, S. Shekhtman, D. Rooney, H. Daly, A modified commercial DRIFTS cell for kinetically relevant operando studies of heterogeneous catalytic reactions, Appl. Catal. A 340 (2008) 196–202.
[4] V. Dal Santo, C. Dossi, A. Fusi, R. Psaro, C. Mondelli, S. Recchia, Fast transient infrared studies in material science: development of a novel low dead-volume, high temperature DRIFTS cell, Talanta 66 (2005) 674–682.
[5] M.V. Martinez-Huerta, G.G. Deo, J.L. Fierro, M.A. Bañaares, Operando Raman-GC study on the structure-reactivity relationship in V^{5+}/CeO2 catalyst for ethane oxidative dehydrogenation: the formation of $CeVO_4$, J. Phys. Chem. C 112 (2008) 11441–11447.
[6] C.M.A. Parlett, C.V. Gaskell, J.N. Naughton, M.A. Newton, K. Wilson, A.F. Lee, Operando synchronous DRIFTS/MS/XAS as a powerful tool for guiding the design of Pd catalysts for the selective oxidation of alcohols, Catal. Today 205 (2013) 76–85.
[7] T. Bürgi, A. Baiker, Attenuated total reflection infrared spectroscopy of solid catalysts functioning in the presence of liquid-phase reactants, Adv. Catal. 50 (2006) 227–283.
[8] U.P. Fringeli, H.H. Günthard, D. Baurecht, in: H.U. Gremlich, B. Yan (Eds.), Infrared and Raman Spectroscopy of Biological Materials, Marcel Dekker, New York, 2000, pp. 143–192.
[9] A. Urakawa, T. Bürgi, A. Baiker, Sensitivity enhancement and dynamic behavior analysis by modulation excitation spectroscopy: principle and application in heterogeneous catalysis, Chem. Eng. Sci. 63 (2008) 4902–4909.
[10] A. Aguirre, A.L. Bonivardi, S.R. Matkovic, L.E. Briand, S.E. Collins, ATR-FTIR study of the decomposition of acetic anhydride on fosfotungstic Wells–Dawson heteropoly acid using concentration-modulation excitation spectroscopy, Top. Catal. 54 (2011) 229–235.
[11] A.G. Young, A.J. McQuillan, Adsorption/desorption kinetics from ATR-IR spectroscopy. Aqueous oxalic acid on anatase TiO_2, Langmuir 25 (2009) 3538–3548.
[12] A. Urakawa, R. Wirz, T. Bürgi, A. Baiker, ATR-IR flow-through cell for concentration modulation excitation spectroscopy: diffusion experiments and simulations, J. Phys. Chem. B. 107 (2003) 13061–13068.
[13] M. Bieri, T. Bürgui, Probing enantiospecific interactions between proline and an L-glutathione self-assembled monolayer by modulation excitation ATR-IR spectroscopy, J. Phys. Chem. B 109 (2005) 10243–10250.
[14] R. Bird, W.E. Stewart, E.N. Lightfoot, Transport Phenomena, second ed., John Wiley, New York, 2002.
[15] PETSc-FEM Home Page. <http://www.cimec.org.ar/petscfem>.
[16] P.A. Kler, C.L.A. Berli, F.A. Guarnieri, Modeling and high performance simulation of electrophoretic techniques in microfluidic chips, Microfluid Nanofluid 10 (2011) 187–198.
[17] Sandia NL, CSimSoft (2000–2009) Paraview: large data visualization. <http://www.paraview.org/>.
[18] N. Kockmann, Transport Phenomena in Micro Process Engineering, Springer, Berlin, 2008.
[19] http://www.octave.org.
[20] Vibrational handbook. J. Chalmers, P.R. Griffiths, (Eds.), Handbook of Vibrational Spectroscopy, vols. 1–5, Wiley & Sons, Chichester, 2001.
[21] H.M. Halvorsen, E. Wygnal, M.R. MacIver, D.G. Leaist, Ternary mutual diffusion coefficients from error-function dispersion profiles: aqueous solutions of Triton X-100 micelles + poly(ethylene glycol), J. Chem. Eng. Data 52 (2007) 442–448.
[22] A. Mialdun, V. Yasnou, V. Shevtsova, A. Königer, W. Köhler, A comprehensive study of diffusion, thermodiffusion, and Soret coefficients of water–isopropanol mixtures, J. Chem. Phys. 136 (2012) 244512–244525.
[23] T. Gervais, K. Jensen, Mass transport and surface reactions in microfluidic systems, Chem. Eng. Sci. 61 (2006) 1102–1121.
[24] R. Hansen, H. Bruus, T.H. Callisen, O. Hassager, Transient convection, diffusion, and adsorption in surface-based biosensors, Langmuir 28 (2012) 7557–7563.
[25] J.Y. Xu, T.W. Chen, W.J. Bao, K. Wang, X.H. Xia, Label-free strategy for in situ analysis of protein binding interaction based on attenuated total reflection surface enhanced infrared absorption spectroscopy (ATR-SEIRAS), Langmuir 28 (2012) 17564–17570.

[26] B. Jin, W.J. Bao, Z.Q. Wu, X.H. Xia, In situ monitoring of protein adsorption on a nanoparticulated gold film by attenuated total reflection surface-enhanced infrared absorption spectroscopy, Langmuir 28 (2012) 9460–9465.
[27] P.A. Suci, M.T. Klem, T. Douglas, M. Young, Influence of electrostatic interactions on the surface adsorption of a viral protein cage, Langmuir 21 (2005) 8686–8693.
[28] T.T. Zheng, Z.X. Sun, X.F. Yang, A. Holmgren, Sorption of phosphate onto mesoporous γ-alumina studied with in situ ATR-FTIR spectroscopy, Chem. Cent. J. 6 (2012) 26–36.
[29] D.E. Mears, Test for transport limitations in experimental catalytic reactors, Ind. Eng. Chem. Prod. DD 10 (1971) 541–547.
[30] M.L. Yarmush, D.B. Patankar, D.M. Yarmush, An analysis of transport resistances in the operation of BIAcore™ implications for kinetic studies of biospecific interactions, Mol. Inmunol. 33 (1996) 1203–1214.
[31] B. Catimel, M. Nerrie, F.T. Lee, A.M. Scott, G. Ritter, S. Welt, L.J. Old, A.W. Burgess, E.C. Nice, Kinetic analysis of the interaction between the monoclonal antibody A33 and its colonic epithelial antigen by the use of an optical biosensor—a comparison of immobilization strategies, J. Chromatogr. A 776 (1997) 15–30.
[32] D. Ferri, T. Bürgui, A. Baiker, Pt and Pt/Al_2O_3 thin films for investigation of catalytic solid-liquid interfaces by ATR-IR spectroscopy: CO adsorption, H_2-induced reconstruction and surface-enhanced absorption, J. Phys. Chem. B 105 (2001) 3187–3195.
[33] S.D. Ebbesen, B.L. Mojer, L. Lefferts, CO adsorption and oxidation at the catalyst–water interface: an investigation by attenuated total reflection infrared spectroscopy, Langmuir 22 (2006) 1079–1085.
[34] A. Bourane, O. Dulaurent, K. Chandes, D. Bianchi, Heats of adsorption of the linear CO species on a Pt/Al2O3 catalyst using FTIR spectroscopy comparison between TPD and adsorption equilibrium procedures, Appl. Catal. A 214 (2001) 193–202.
[35] A.W. Adamson, Physical Chemistry of Surfaces, fifth ed., John Wiley & Sons Inc., New York, 1990.